Structure characteristics and mechanical properties of kaolinite soils. I. Surface charges and structural characterizations

Y.-H. Wang and W.-K. Siu

Abstract: In this study on the surface charges and structural characterization of kaolinite clay, it is found that the highly pH dependent edge charges are important to the interparticle forces and associated fabric formations. When the pH is below the isoelectrical point of the edge surfaces, IEP_{edge}, the Coulombian attraction between faces and edges dominates, which favors the formation of an opened edge-to-face (EF) association and a higher final sediment volume. At pH > IEP_{edge}, the double-layer repulsion prevails at all surfaces to result in a deflocculated and dispersed fabric, which tends to form denser soil packing in the sediment. Increasing the ionic strength (with NaCl as the electrolyte) leads to the opposite behavior in clay suspensions below and above the IEP_{edge}: the degree of fabric flocculation and the final sediment volume decrease with an increased ionic strength at pH < IEP_{edge} but increase at pH > IEP_{edge}. The measured pore-size distribution reveals a distinct dual-porosity characteristic in the pH 4 with salts (0.15 mol/L NaCl) specimen: it consists of inter-aggregate spaces (~1.10 μm) and intra-aggregate pores (~0.30 μm). Soils with a higher degree of EF flocculation due to the prevailing Coulombian or van der Waals attraction can render a higher liquid limit.

Key words: pH, fabric associations, isoelectrical point, dual porosity, interparticle forces, liquid limit.

Résumé : Dans cette étude des charges de surface et de la caractérisation structurale de l'argile de kaolinite, on a trouvé que les charges aux arêtes qui sont fortement dépendantes du pH sont importantes pour les forces interparticules et les formations associées de fabriques. Quand le pH est sous le point isoélectrique des surfaces d'arête, IEP_{edge}, l'attraction Coulombienne entre les faces et les arêtes domine, ce qui favorise la formation d'une association ouverte arête-face (EF) et d'un volume final plus élevé de sédiments. À un pH > IEP_{edge}, la répulsion de la double couche domine sur toutes les surfaces pour donner naissance à une fabrique défloculée et dispersée, ce qui tend à former un assemblage de sol plus dense dans le sédiment. L'accroissement de la force ionique (avec NaCl comme électrolyte) mène à un comportement opposé dans les suspensions d'argile sous ou au-dessus du IEP_{edge} : le degré de floculation de la fabrique et le volume final de sédiment diminuent avec un accroissement de la force ionique à un pH < IEP_{edge}, mais ils s'accroissent à un pH > IEP_{edge}. La mesure de la porosimétrie révèle une caractéristique distincte de porosité double à un pH de 4 avec un spécimen de sels (0.15 mol/L NaCl) : elle consiste en des espaces inter-aggrégats (~1,10 μm) et des pores intra-agrégats (~0.30 μm). Les sols ayant un plus haut degré de floculation EF dû à l'attraction Colombienne ou de van der Waals prévalente peut produire une limite liquide plus élevée.

Mots clés : pH, associations de fabriques, point isoélectrique, porosité double, forcces interparticules, limite liquide.

[Traduit par la Rédaction]

Introduction

The behavior of fine-grained soils, especially those with higher specific surfaces, is intimately related to the properties of the pore fluid because of the charged surfaces and associated interparticle forces. The pore-fluid properties of soils can be altered due to various events, such as contamination by solid and (or) liquid waste, seawater invading a freshwater environment, or marine deposits flushed with rainwater (Mitchell 1993; Evans 1990). In response to these events, the interparticle force and fabric arrangement of soils tend to vary, which in turn regulates their engineering properties, such as hydraulic conductivity, compressibility, stiffness, and strength (Sridharan and Rao 1979; Fernandez and Quigley 1985; Mitchell 1993; Chen et al. 2000; Santamarina et al. 2001). The proposed underlying mechanisms for these changes are usually attributed to the combined effects of double-layer repulsion and van der Waals attraction between negatively charged face sites of clay particles (i.e., Derjaguin–Landau–Verwey–Overbeek (DLVO) forces). Such a simple conclusion sometimes leads to contradictions, however, especially when considering kaolinite clay. For instance, the *S*-wave velocity of kaolinite decreases with increasing ionic strength, which is in opposition to the consequence of reducing the double-layer repulsion (see the test data in Santamarina and Fam 1995). This contradiction is the result of ignoring the influence of the edge surface charges. The

Received 23 November 2004. Accepted 10 March 2006. Published on the NRC Research Press Web site at http://cgj.nrc.ca on 23 May 2006.

Y.-H. Wang[1] and W.-K. Siu. Department of Civil Engineering, Hong Kong University of Science and Technology, Clear Water Bay, Kowloon, Hong Kong.

[1]Corresponding author (e-mail: ceyhwang@ust.hk).

 doi:10.1139/T06-026

Fig. 1. Mineral compositions and surface charge characteristics of kaolinite (based on Parks 1967; Huang and Stumm 1973; Ferris and Jepson 1975; Jepson 1984; Zhou and Gunter 1992; Braggs et al. 1994; Ma and Eggleton 1999; and Carty 1999).

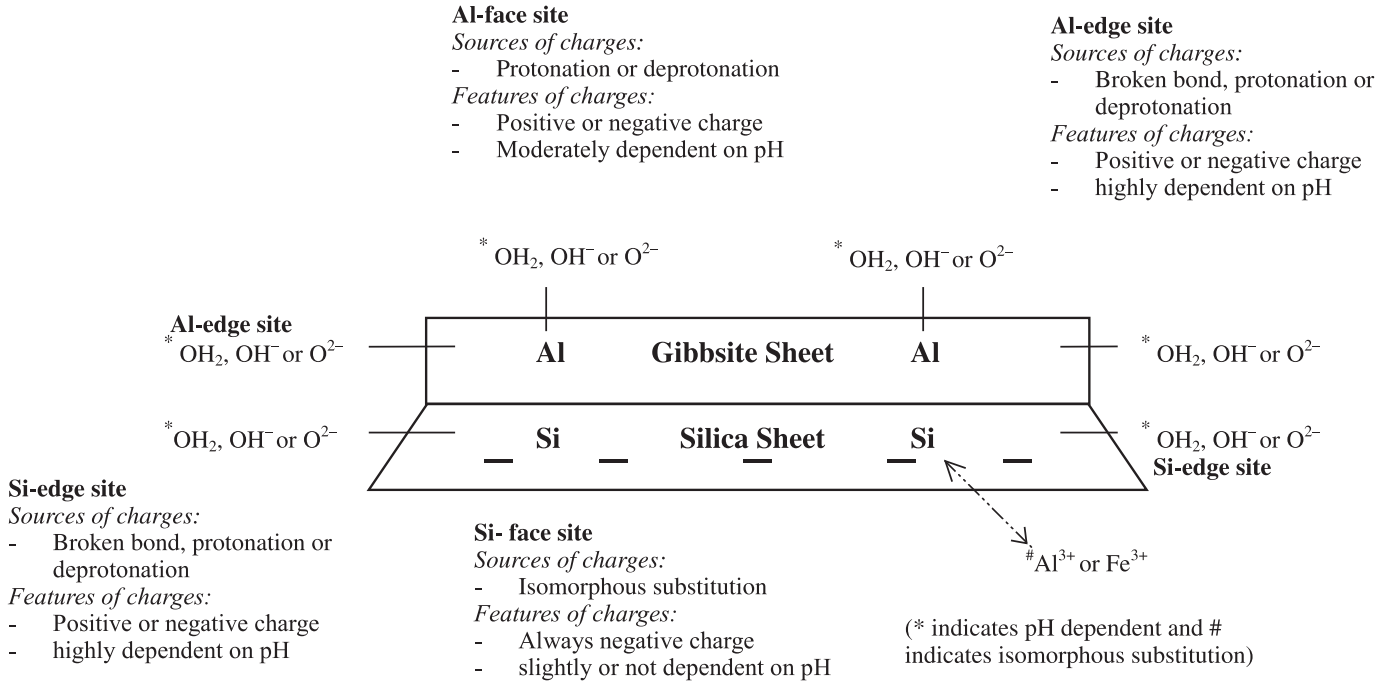

portion of edge surface areas in kaolinite is higher than that of the common view, and therefore its significance should be considered (Brady et al. 1996; Zbik and Smart 1998). In this context, highly pH dependent edge surface charges and the associated interparticle forces of edge-to-face (EF) should be studied to fully understand chemical–mechanical coupling in kaolinite.

Guided by the earlier studies, this paper was designed to systematically elucidate the features of the surface charges and associated fabric formations of kaolinite under different pH and (or) ionic strengths. It begins with a review of the fundamental concepts related to surface charges, interparticle forces, and fabric associations. The results of fabric characterizations of various pH and ionic strengths using various methods are discussed and compared. Moreover, the relevance of the interparticle electrical force to the liquid and plastic limits is revisited in depth. The companion paper focuses on the influence of structure on the mechanical properties of kaolinite.

Characteristics of surface charges

Different types of surface charges contribute to the total particle surface charges of clay minerals. These types include permanent structural charges caused by isomorphic substitutions or broken bonds in minerals, θ_0, which are always negative; the charge due to the binding of protons of H^+ or OH^-, θ_H, which can be either positive or negative; and the adsorbed ion charge within the stern layer, θ_{stern}, which depends on the concentration, valence, and size of the ions (Stumm 1992; Sposito 1998):

$$[1] \qquad \theta_p = \theta_0 + \theta_H + \theta_{stern}$$

By electrical neutrality, the net surface charge, θ_p, is balanced by counter charges in the diffused swarm, θ_D. Changing the pH can result in a positive or negative θ_p; under certain circumstances, there is a zero θ_p for which the pH value is referred to as the point of zero charge (PZC). The PZC is very close to the isoelectric point (IEP), where the zeta potential is zero, but not identical due to the entrapment of diffused ions within the shear plane (Sposito 1998). These definitions of PZC and IEP correspond to the whole particle. Actually, different sensitivities of the edges and faces to protonation and complexation can lead to distinguishable PZC and IEP for edges and faces.

Surface charges and associated fabric formations of kaolinite

Mineralogy and surface charge characteristics of kaolinite

Kaolinite is a 1:1 dioctahedral aluminosilicate with two basal cleavage faces: an alumina octahedral sheet and a silica tetrahedral sheet (Hurlbut 1971; Carty 1999). These two sheets are tightly bound by sharing oxygen atoms. Between layers, the bonding is primarily electrostatic, augmented by van der Waals forces and hydrogen bonds (Plancon et al. 1989; Mitchell 1993). In the absence of interlayer cations in kaolinite, interlayer swelling as observed in montmorillonite is not possible. At the edges, the exposed Al and Si are usually terminated by hydroxyl groups (Schofield and Samson 1954).

There is no universally accepted interpretation about the surface charges of kaolinite because the charge sites vary with different chemical compositions or defect structures (Brady et al. 1996). Figure 1 summarizes the features of the surface charges on the basal surface site and the edge site.

Fig. 2. Sign of charges at the edge sites under different pH values (modified from Braggs et al. 1994).

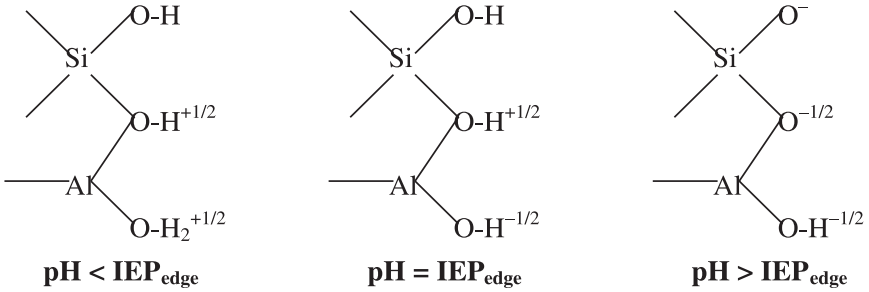

Table 1. Values of the isoelectric point (IEP) and point of zero charge (PZC) of the edge surface of kaolinite.

Sample	Technique	IEP	PZC	Reference
Monoionic Na kaolinite	Na^+, H^+, Cl^- adsorption	—	7	Flegmann et al. 1969
Monoionic Na kaolinite	Rheology	5.8	—	Flegmann et al. 1969
Monoionic Na kaolinite	Dynamic light scattering	5.7	—	Kretzschmar et al. 1998
Commercial kaolinite	Sedimentation	5.8	—	Dollimore and Horridge 1972
Monoionic Na kaolinite	Rheology	7.3±0.2	—	Rand and Melton 1977
Hydrite PX kaolinite from Georgia Kaolin Company	Rheology and sedimentation	5.25	—	Braggs et al. 1994

The details of these features are given in the following subsections.

Face charge

Due to isomorphous substitution of Si^{4+} by Al^{3+} or Fe^{3+} in the tetrahedral sheet, a permanent (non-pH dependent) negative charge on the Si basal surface arises (Schofield and Samson 1954; Bolland et al. 1980; van Olphen 1991). The octahedral gibbsite consists of hydroxyl groups on the surface. These hydroxyl groups render pH-dependent charges, but they are less reactive compared to those on the edge sites. Carty (1999) proposed that kaolinite particles possess a dual basal surface for which the silica-like surface is negatively charged and the alumina-like surface is positively charged at pH ranging from 3.5 to 8.5. This inference is based on the colloidal behavior of silica in which the IEP is 2.0–3.5 and that of alumina in which the IEP is 8.5–10.4. Nevertheless, in general, the overall surface charge on the basal planes is always considered to be negative, but the magnitude is pH dependent (Jepson 1984; Zhou and Gunter 1992; Ma and Eggleton 1999).

Edge charge

The broken edges are widely regarded as major reactive sites with potential determining ions, such as H^+ and OH^- (Wierer and Dobias 1988). Therefore, changing pH primarily affects the charge on the edge site rather than on the basal surface site. The dual edge surface was also posited by Huang and Stumm (1973) and Parks (1967): the signs of the surface charge of aluminol and silanol on the edge sites may be opposite at certain pH; the positive edge charge is mainly contributed by the aluminol edge sites (Ferris and Jepson 1975). The variation in charges at these two locations around the edge IEP (IEP_{edge}) is shown in Fig. 2. Still, it is in general simply assumed that these two types of edge sites have a charge of the same sign at any pH. Moreover, the charge is converted from positive to negative when the pH exceeds the IEP or PZC of the edge site, IEP_{edge} or PZC_{edge}. The published PZC of kaolinite edge surfaces ranges from pH 5 to pH 9, varying with different types of kaolinites, pretreatment processes, and the method adopted for its determination (reviewed by Kretzschmar et al. 1998). Table 1 summarizes some of these data, including the determination method.

Summary

The face charge (on the basal plane) is always negative and slightly pH dependent, whereas the edge charge can be either positive or negative, effectively depending on the pH. For kaolinite, the portion of edge surfaces is high, about 12%–34% (Ferris and Jepson 1975; Brady et al. 1996; Zbik and Smart 1998), and the face charge due to isomorphic substitution is not severe (van Olphen 1991; Brady et al. 1996). Hence, the pH effects are important to the behavior of kaolinite, and the significance sometimes can overwhelm the influence of ionic strength when the cation concentration is low to moderate (Braggs et al. 1994).

Interparticle forces and fabric associations

There are three main electrical forces controlling the fabric associations of kaolinite: van der Waals attraction, double-layer repulsion, and Coulombian electrostatic forces. The summation of the first two is the so-called DLVO force. The subtle balance between these three forces occurring between different sites (i.e., edges or faces) can lead to various modes of particle associations (Fig. 3): edge-to-face (EF) flocculation, edge-to-edge (EE) flocculation, face-to-face (FF) aggregation, and dispersed–deflocculated fabric (van Olphen 1991). Note that different particle associations also can link up as a continuous network to form a card-house structure while they are flocculated.

Bingham yield stress

Different particle associations can also lead to various Bingham yield stresses of kaolinite suspensions, modulated by the interparticle forces (Rand and Melton 1977; Ma and Pierre 1999). The yield stress varies with variation in pH and

Fig. 3. Particle associations in kaolinite (modified from van Olphen (1991) and Santamarina et al. (2001)).

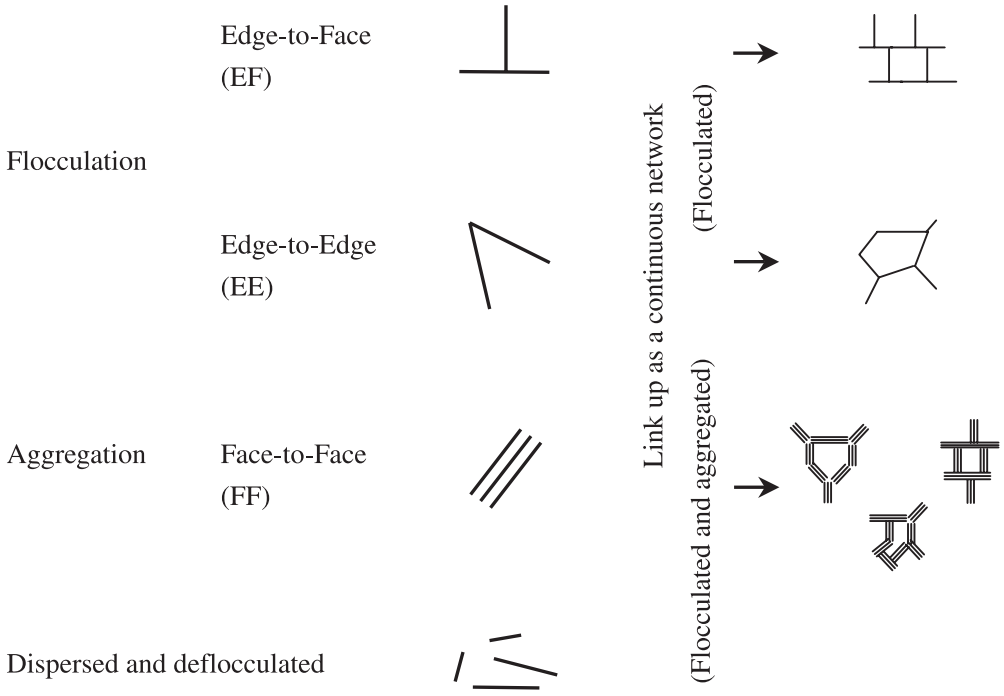

ionic strength as illustrated in Fig. 4. Important observations from Fig. 4, and proper interpretations, following Rand and Melton (1977), are summarized as follows:

(1) At pH > IEP_{edge}, the edge and face are negatively charged, so double-layer repulsion prevails, which in turn renders a dispersed–deflocculated structure and a lower yield stress. While at pH < IEP_{edge}, the EF flocculation prevails because of Coulombian attraction between oppositely charged face (negative) and edge (positive), leading to stronger interparticle forces and a higher yield stress. At pH ≈ IEP_{edge}, a transition fabric formation, EE association, is suggested.

(2) The yield stress decreases with increasing electrolyte concentration, *c*, at pH < IEP_{edge}. This is because the addition of NaCl at pH < IEP_{edge} compresses the double layers at both edge and face sites (positive and negative double layers, respectively) and reduces their effective Coulombian attraction, which in turn weakens the formation of the EF flocculated structure and the yield stress. In the meantime, the FF aggregation is promoted due to a reduction in the repulsion between faces. At pH > IEP_{edge}, however, the increase in the electrolyte concentrations gradually increases the yield stress because a reduction in the double-layer repulsion (negative double layers at all sites) promotes van der Waals attraction for coagulation: an aggregated and flocculated structure forms.

Fig. 4. Variation in the yield stress as a function of pH (modified from Rand and Melton (1977) and Low (1991)).

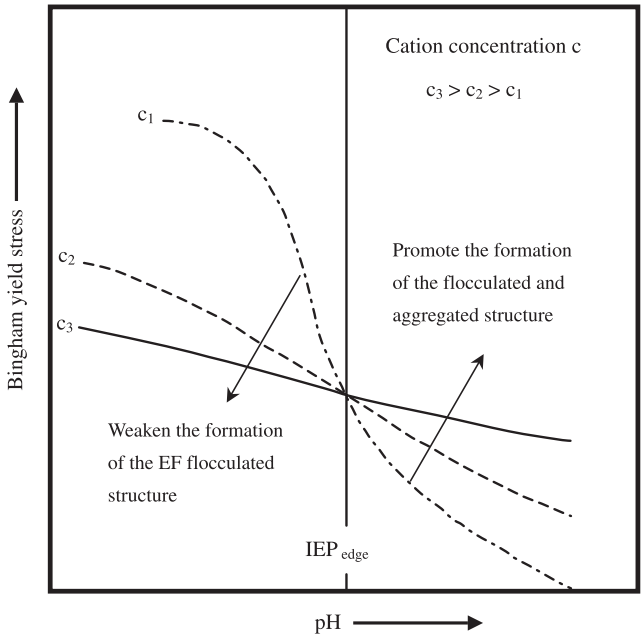

Sediment volume

The interparticle force and associated fabric formations also can lead to different sediment volumes. As illustrated in Fig. 5*a*, by the aid of the potential barrier to coagulation or the interparticle repulsion, the particles in the suspension with deflocculated structures are able to slide and roll over each other when reaching the lower part of the sediment tube. Consequently, the particles can be rather closely packed like the FF alignment, and a dense sediment is formed. Flocculated structures such as EF and EE associations, however, can resemble a continuous network (a cardhouse structure) to form a voluminous sediment (Fig. 5*b*). Consequently, a higher sediment volume should be observed for a kaolinite suspension when a strong Coulombian attraction between edges and faces dominates, i.e., a higher degree of EF flocculation (Lambe 1958; Dollimore and Horridge 1972; Sridharan et al. 1988; van Olphen 1991).

Fig. 5. A schematic diagram of fabric packing in the sediment: (*a*) dispersed and deflocculated structure; (*b*) flocculated structure (modified from van Olphen 1991).

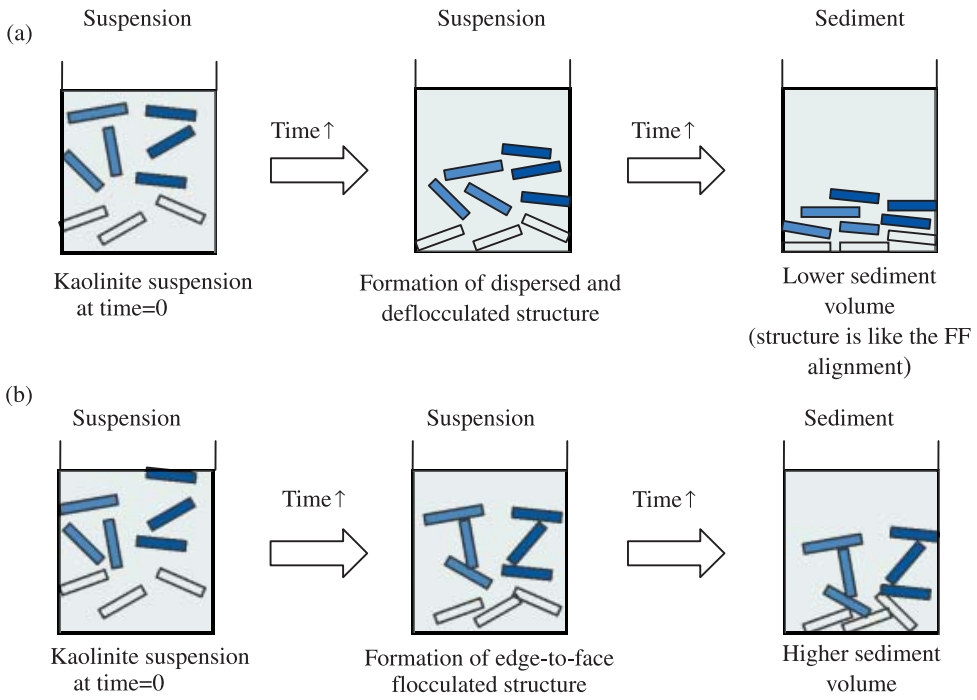

Effects of the state of stress

Apart from the interparticle forces associated with the pore fluid of different chemical properties, the clay fabric can also be regulated by the state of stress. Experimental observations and numerical simulations reveal that the clay particles tend to align along the major principal stress plane as a higher vertical effective stress is applied during one-dimensional (1D) consolidation (Hicher et al. 2000; Yao and Anandarajah 2003). Moreover, the higher effective stress acting on a clay liner can help preserve its low hydraulic conductivity against chemical attack because the fabric is controlled by the state of the stress rather than by interparticle electrical forces (Fernandez and Quigley 1985; Broderick and Daniel 1990). In this context, fabric characterizations should be conducted not only at the deposition stage, but also at the stage after the clay has been subjected to a certain amount of loading, which is more relevant to the general practice of geotechnical engineering.

Materials and sample preparation

The soil used in this study is Speswhite Kaolin and consists of 47% SiO_2 and 38% Al_2O_3. The specific gravity and surface area (Brunauer–Emmett–Teller (BET)) are 2.6 and 14 m^2/g, respectively. The particle size is mostly smaller than 2 μm, and the pH value is about 5 ± 0.5. Table 2 summarizes the mineralogy and properties of Speswhite Kaolin.

Table 2. Mineralogy and properties of Speswhite Kaolin (provided by Imerys Minerals Ltd., UK).

SiO_2 (%)	47
Al_2O_3 (%)	38
Grain size (%)	
300 mesh residue	0.02 (max.)
≥10 μm	0.5 (max.)
≤2 μm	80±3
Specific gravity	2.6
Surface area (BET, m^2/g)	14
pH	5.0±0.5
Oil absorption	42 g per 100 g
Water-soluble salts content (%)	0.2

Pretreatment

As excess salts and impurities are present in clay powders, pretreatment by a series of washing steps is required. A large amount of deionized water was first mixed thoroughly with dry clay powder to form a clay suspension, which was then allowed to settle for 3 to 4 days. The supernatant liquid above the kaolinite sediment was siphoned off, and the sediment was remixed with fresh deionized water. After repeating the aforementioned procedure six times, the washing was considered completed and a great drop in conductivity was detected as shown in Table 3, indicating that the excess salts had been removed to a stable condition, and the soil could be considered electrolyte free. This state is referred to as the point of zero electrolyte concentration in the following discussions.

Adjusting pore-fluid properties

After the washing pretreatment, the electrolyte-free clay slurry was adjusted to different pH values and electrolyte concentrations according to the experimental design. The pH value was modulated by adding either 0.05 mol/L hydrochloric acid (HCl) or 0.2 mol/L sodium hydroxide (NaOH) until the target pH was reached. The electrolyte concentration was adjusted by adding sodium chloride (NaCl). The re-

Table 3. Electric conductivity and equivalent NaCl concentrations of clay suspensions versus washing steps.

Washing step	Electric conductivity (μs/cm)	Equivalent NaCl concentration (mol/L, $\times 10^{-3}$)
0	650	7.11
1	506	5.54
2	429	4.69
3	329	3.60
4	253	2.77
5	162	1.77
6	119	1.30
7	100	1.09

Note: Total dissolved solids (in mg/L) ≅ 640 × electric conductivity (in dS/m), as proposed by Rhoades (1996). Equivalent NaCl concentration = (total dissolved solids)/(molar mass of NaCl).

quired amount of NaCl salt was first dissolved in a small amount of deionized water, and then this salt solution was thoroughly mixed with the clay slurry. Note that all the chemicals used were purposely chosen to obtain a suspension with monovalent ions.

One-dimensional consolidation

The clay slurry with assigned pH and (or) ionic strength was carefully poured into a consolidometer to avoid the entrapment of air bubbles. The bubbles were also effectively removed by slowly stirring the slurry layer by layer inside the consolidometer. A vertical pressure of 100 kPa was applied for 1D consolidation. When the vertical settlement converged to a steady value, the consolidation was considered to be finished. After the consolidation was completed, samples were trimmed for scanning electron microscopy (SEM) imaging, pore-size measurements by mercury intrusion porosimetry (MIP), and Atterberg limit tests.

Experimental details

Three tests were performed to characterize the soil fabric at the deposition stage: the sedimentation test and 1D consolidation to 100 kPa to measure the pore-size distribution by MIP and SEM imaging. Also, Atterberg limit tests were conducted to consider the relevance of the interparticle forces and fabric associations.

Sedimentation test

A sedimentation test is the simplest way to characterize particle interactions and associated fabric formations at the deposition stage under a very low state of stress. In this test, 10 g of kaolin powder was mixed with 45 mL of deionized water in a test tube. The initial sediment void ratio was calculated as 10.7. The pretreatment stage, six washing steps, was implemented before the test. Suspensions under the electrolyte-free condition with pH ranging from 2 to 9 were prepared to observe the pH effect. Suspensions with different electrolyte concentrations ranging from 0.005 to 1 mol/L were prepared to assess the effect of ionic strength for soil suspensions at two representative pH values (i.e., pH 4 and pH 7.8). Since the interparticle electrical force can influence the initial settling rate and the final sediment volume of a clay suspension, both quantities were continuously recorded over time. Note that the mechanical disturbance was minimized as the test proceeded.

Measurement of pore-size distribution: mercury intrusion porosimetry (MIP)

After consolidation, the sample was carefully trimmed into a small cube with dimensions of ~1.0 cm × 1.0 cm × 0.5 cm. The trimmed samples were immediately placed in liquid nitrogen for quick freezing of their pore fluids, which were directly sublimed (freeze-drying method) to prevent fabric alteration due to capillary effects. About 1.5 g of specimen was used for the MIP test.

The MIP test was carried out using a Micromeritics AutoPore IV 9500 V1.04 with a maximum intrusion pressure of 210 MPa. The pore-size distribution is determined based on the theory that a nonwetting fluid can intrude the voids of a porous material of a size inversely proportional to the fluid pressures. The intrusion pressure, P, and the pore diameter, D (assuming a right cylinder of constant radius), are related by the following equation:

$$[2] \qquad D = -4\gamma \cos\theta / P$$

where γ is the surface tension of mercury (485 dynes/cm at room temperature), and θ is the contact angle (Washburn 1921). The advancing and receding contact angles, 162° and 158°, respectively, determined by Penumadu and Dean (2000) for kaolinite are used here. Note that, as discussed by Griffiths and Joshi (1989), the derived value is an equivalent cylindrical diameter because of the irregularity of clay pores.

Scanning electron microscopy (SEM) imaging

Scanning electron microscopy provides direct observations of the fabric associations in kaolinite. The freeze-drying method was also used in these sample preparations. Before taking the SEM images, gold-coating pretreatment was implemented. The images were taken by a JSM-6300 scanning electron microscope. Note that the sample surface is unpolished to preserve the fabric.

Atterberg limits

The British Standards Institution (1990) cone penetrometer method BS1377 (Part 2: 1990: 4.3) was used to determine the liquid limit of the samples. The plastic limit (PL) was determined by finding the water content at which a soil thread with a 3.2 mm diameter just crumbles, as described by the American Society for Testing and Materials (ASTM 1995) test method D4318-95a and British Standards Institution (1990) method BS1377 (Part 2: 1990: 5.3). Note that a solution with the same chemical properties as those of the soil pore fluid is used instead of deionized water while the soil sample has to be remixed with different water contents, thereby preventing leaching effects.

Experimental results and discussion

Sedimentation test

Before looking at the details of the experimental results, the factors controlling the settling rate of the suspension are discussed. Stokes law indicates that the settling velocity, v, for a spherical particle is a function of the spherical diame-

Fig. 6. Rates of void ratio changes as a function of pH (sedimentation time = 2 h).

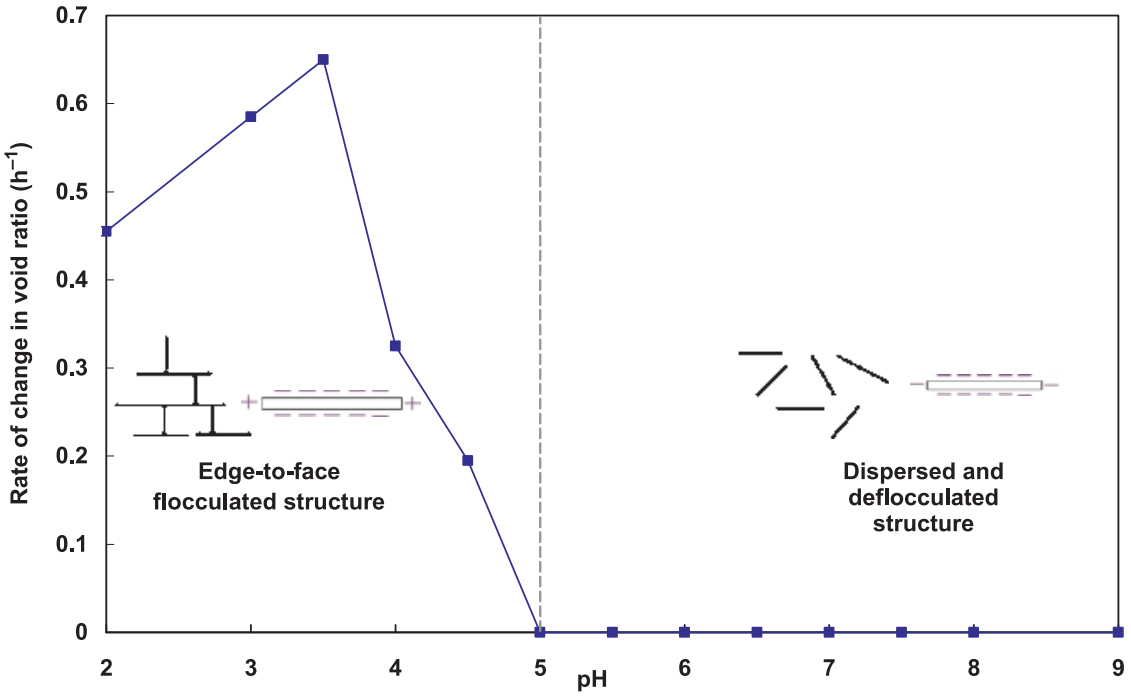

ter, D, the fluid viscosity, μ, and the difference in the specific weight of the sphere and the fluid, $G_s - G_f$:

$$[3] \qquad v = \frac{(G_s - G_f)\gamma_w}{18\mu} D^2$$

where γ_w is unit the weight of water. It is believed that these three factors also affect the settling rate of clay particles, although the particle shape is platy. Since no particle interaction is assumed in Stokes law, the electrical forces between clay particles should be added as an important factor to the behavior of a clay suspension, as suggested by Chamley (1989) and Toorman (1996). Chambly and Toorman also pointed out that the particle concentration, n, and the size of the container, S, are the other supplementary influential factors: an increase in the particle concentration induces a greater hindrance, and a smaller container size causes higher wall friction, which both result in a lower settling rate. Guided by the previous discussions, the initial settling rate for a kaolinite suspension is proposed to be a function of the conglomerate size, D; the fluid viscosity, μ; the difference in the specific weight of the clay particle and fluid, $G_s - G_f$; the net particle interaction force, $A - R$ (the attractive force minus the repulsive force); the particle concentration; and the size of the container; as shown by

$$[4] \qquad \text{settling rate} = f(D,\ 1/\mu,\ G_s - G_f,\ A - R,\ n,\ S)$$

In the experiment performed here, only D and $A - R$ are not controlled. Moreover, the conglomerate size is determined by the interparticle forces (Low 1991). Consequently, the difference in settling rates can be mainly attributed to the interparticle forces. When the interparticle attractive force prevails, coagulation is promoted to accelerate suspension settlement.

Figure 6 shows the rate of change in the void ratios during the first 2 h (i.e., the average initial settling rate) for the kaolinite suspensions with different pH values. The rate increases from pH 2 to pH 3.5 and then decreases at pH above 3.5. No change in the void ratio is observed at pH 5 or above, however. This result implies that the attractive force between the particles overwhelms the repulsion force at a pH below 5. The Coulombian attraction prevails because the edge site becomes positive due to protonation in the acidic environment. The decreasing trend found at pH lower than 3.5 can be explained by the effect of the chloride anions bound to the positively charged edges, which somehow hinder the EF association. Note that HCl is used in the test to lower the pH. The higher pH converts the edge charge to negative. Hence, all the surfaces (face and edge) now are negatively charged and the prevailing repulsive force increases the energy barrier between the particles, which in turn prevents coagulation.

The time required to detect the settlement can better reveal the pH effects (Table 4). It can be seen that the energy barrier for conglomeration increases with increasing pH. As mentioned previously, the acidic environment enhances the positive charge density of the edges, which in turn facilitates the EF Coulombian attraction to prevail. On the other hand, increasing the pH adds negative charges to both edge and face sites. The consequence of this is to increase the interparticle repulsion force and reduce the number of particles that stick together in each particle collision. Note that the result also indicates that pH 5 is a transition point to separate different settling behaviors.

Figure 7 presents the final sediment volume (in terms of the void ratio) of the kaolinite suspensions with different pH values. The final void ratio of the suspension below pH 5 is about two times higher than that for the suspensions at and above pH 5. This suggests that distinct fabrics are formed

Fig. 7. Final sediment volumes of the suspensions as a function of pH (sedimentation time = 4 months).

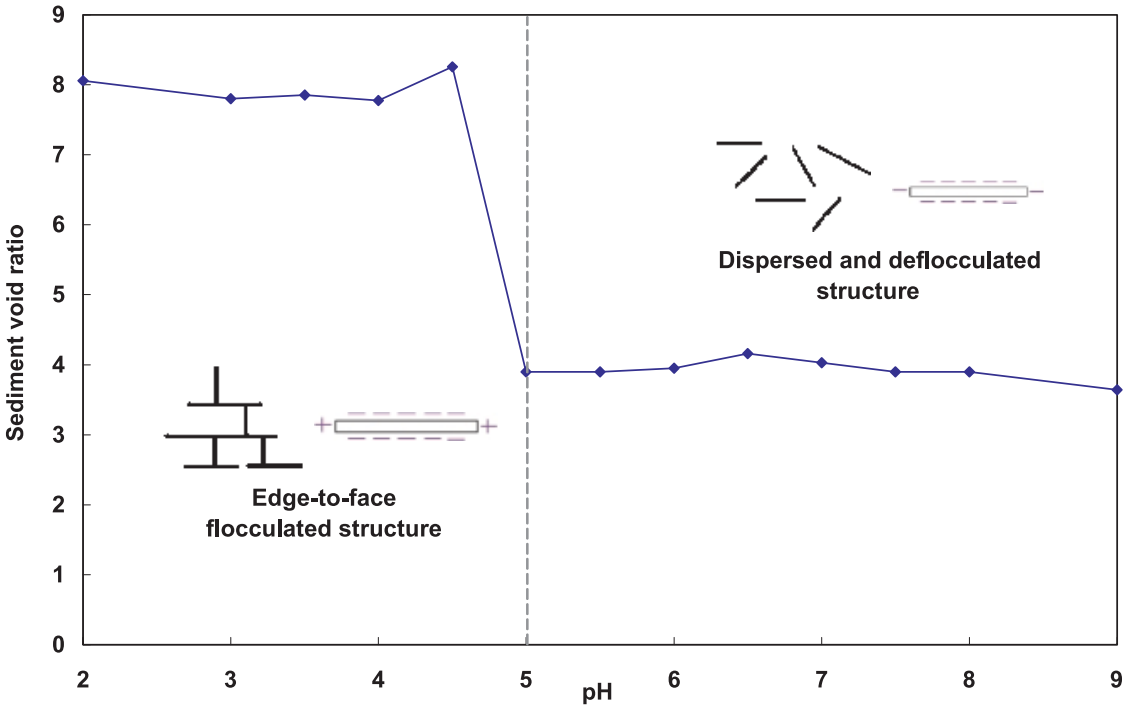

Table 4. Time required to detect the settlement.

pH	Time required (h)
2.0	0.5
3.0	0.5
3.5	0.5
4.0	1.0
4.5	1.0
5.0	85.0
5.5	85.0
6.0	85.0
6.5	85.0
7.0	121.0
7.5	121.0
8.0	147.0
9.0	147.0

below and above this transition pH: the fabric changes from a card-house network to a closely packed structure when the pH value exceeds 5. According to the previous discussion, it can be inferred that the surface charge changes from positive to negative on the edge site at ~pH 5, which is therefore simply estimated as the isoelectric point of the edge site (IEP_{edge}).

Following the previous analysis, pH 5 seems to be a boundary for the fabric transition. Hence, a study of the effect of ionic strength is selected for soil suspensions with pH above and below this boundary (pH 4 and pH 7.8). At pH 4, the edge (positive) and face (negative) are charged with an opposite sign; at pH 7.8, the edge and face are negatively charged. Figure 8 shows the change rates of the void ratios (i.e., the average initial settling rate) as a function of ionic strength. In the pH 7.8 suspension, the addition of a small amount of electrolyte can dramatically increase its settling rate until the concentration exceeds 0.15 mol/L. Beyond this concentration there is little change in the average settling rate. Increasing the ionic strength compresses the double layers at the faces and edges. Hence, both the FF aggregation and also the linkup of such associations in the EF and EE fashion are promoted. That is, the prevailing van der Waals attraction between all surfaces of the face and edge sites enhances coagulation and the settling rate. The behavior of pH 4 suspension is discussed together with the final sediment volume next.

The corresponding sediment volume is presented in Fig. 9, which shows that adding only a small amount of electrolyte (NaCl) can significantly increase the final sediment volume of the pH 7.8 suspension. This is because of the promotion of the flocculated and aggregated structure. Such an increasing trend contradicts some published results (e.g., Chen and Anandarajah 1998; Fam and Dusseault 1998). A comparison with data presented in the literature must consider pH effects, however. The pH of an untreated kaolinite suspension is usually below the IEP_{edge}. The published results should therefore not be applicable to the pH 7.8 specimen of this study and yet should be in accordance with results for the pH 4 specimen: the final sediment volume decreases with increasing electrolyte concentration from 0.01 to 0.50 mol/L. The addition of NaCl at pH < IEP_{edge} compresses the positive double layers at the edges and the negative double layers at the faces, which in turn reduces their mutual Coulombian attraction. This action weakens the formation of the EF flocculated structure and reduces the sediment volume. Note that slight increases in the sediment volume and the average settling rate are observed when the concentration increases from the electrolyte-free condition to 0.01 mol/L at pH < IEP_{edge}, and the underlying mechanisms need further clarification. At concentrations greater

Fig. 8. Effects of NaCl concentration on the average initial settling rate of pH 4 and pH 7.8 specimens (sedimentation time = 2 h).

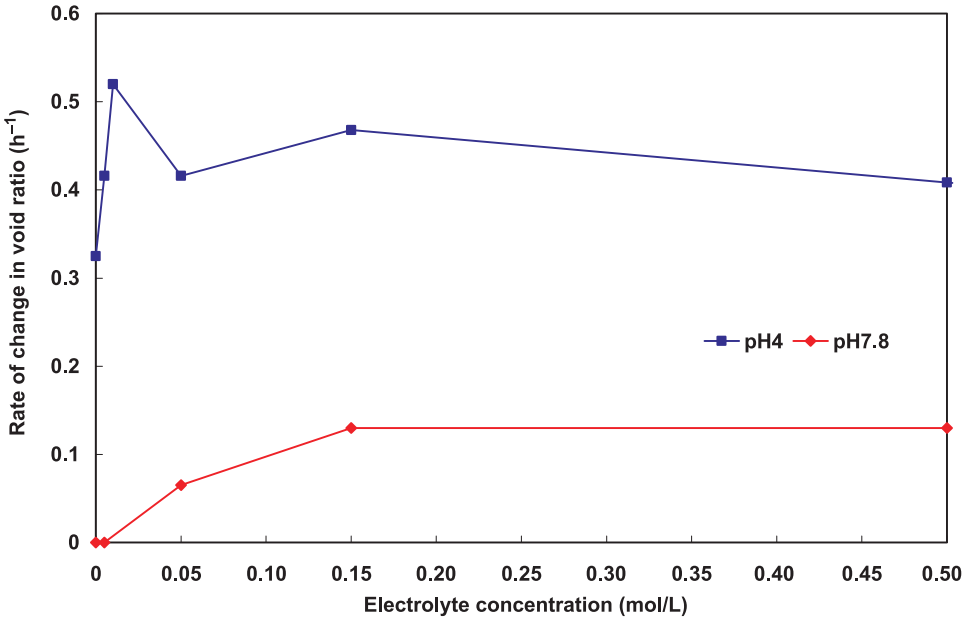

Fig. 9. Effects of NaCl concentration on the final sediment void ratio of pH 4 and pH 7.8 specimens (sedimentation time = 4 months).

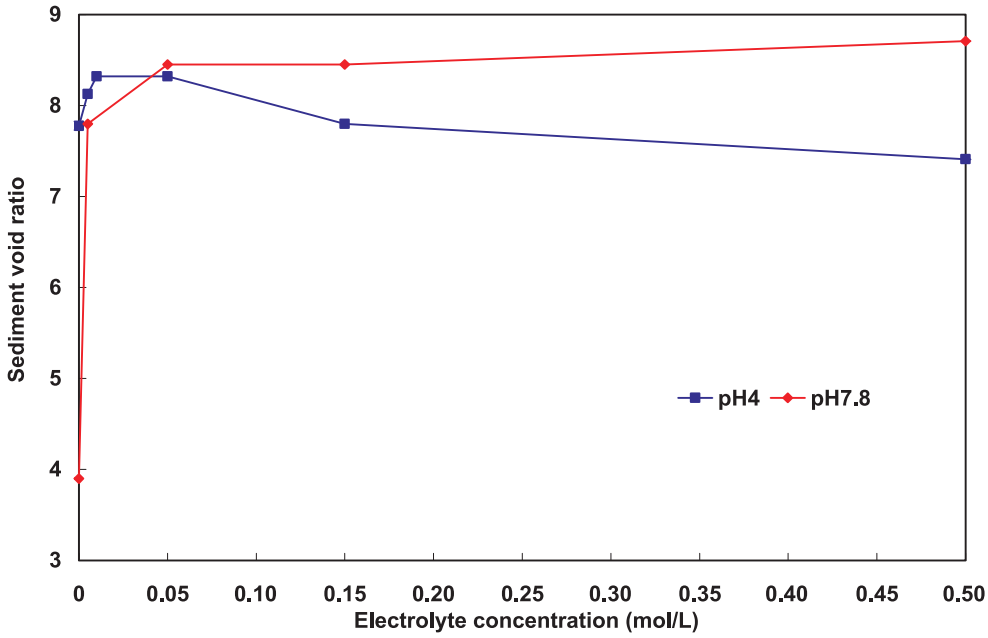

than 0.01 mol/L, the settling rate of the pH 4 suspension is not obvious in reflecting the deterioration of the EF association as shown in the sediment volume. The above discussion explains the contradiction mentioned in the Introduction that the *S*-wave velocity of kaolinite deceases with an increase in ionic strength: fewer EF associations lower the stiffness of the soil. Further direct evidence can be found in the companion paper.

Scanning electron microscopy

Figures 10, 11, and 12 are SEM images of the kaolinite specimens at pH 4, pH 7.8, and pH 4 with an electrolyte concentration of 0.15 mol/L. For the pH 4 specimen with and without the addition of salt, both the EF flocculated fabric, as expected, and the FF aggregated fabric are readily seen. Indeed, calculations show that EF and FF associations can occur simultaneously even for faces and edges having electric charges of opposite signs (Flegmann et al. 1969). Furthermore, FF aggregation can be promoted after the electrolyte concentration is increased to decrease the double-layer repulsion (Fig. 12). It should be noted, however, that the FF association is not uniformly packed as shown in Fig. 10. The irregularities of particle shapes, sizes, packing, and orientation certainly help enlarge the pore size within the FF association. As a result, the pore size within FF aggregation is larger than the estimate based exclusively on the

Fig. 10. SEM image of the pH 4 specimen. ○, edge-to-face aggregation; △, face-to-face aggregation.

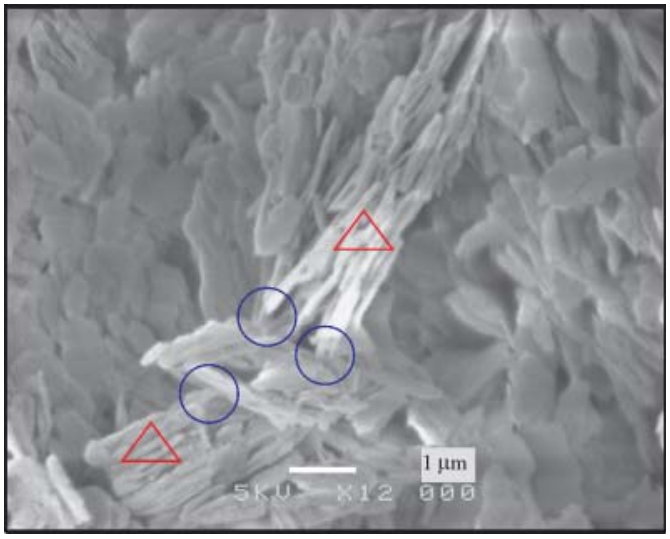

Fig. 11. SEM image of the pH 7.8 specimen.

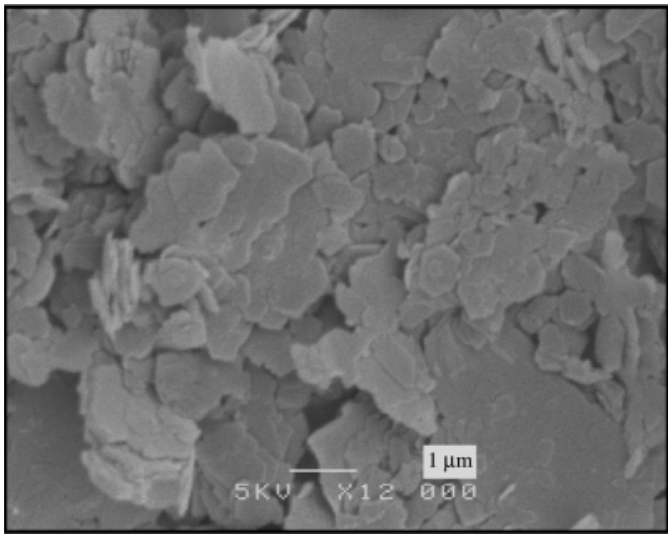

working range of the double-layer theory, ~10 nm. For the pH 7.8 specimen, the particles are oriented in the same direction and no significant flocculation is observed, which is consistent with the observation of the sedimentation test.

Mercury intrusion porosimetry (MIP)

Figure 13 presents the pore size versus intruded volumes for specimens with two different fabrics. The total intruded volume (per gram) of the pH 7.8 specimen (Fig. 13*a*) is much lower than that due to the denser packing formed (FF alignment). This result also implies that the open card-house structure (flocculated and aggregated) in the pH 4 with salts (0.15 mol/L NaCl) specimen can be sustained after being subjected to the 1D consolidation of 100 kPa. As shown in Fig. 13*b*, the predominant pore diameter of the pH 7.8 specimen is about 0.27 μm, which represents the main pore size of soils with the FF alignment (association). The pH 4 with salts specimen shows a predominant pore diameter of

Fig. 12. SEM image of the pH 4 specimen with 0.15 mol/L electrolyte concentration. ○, edge-to-face flocculation; △, face-to-face aggregation.

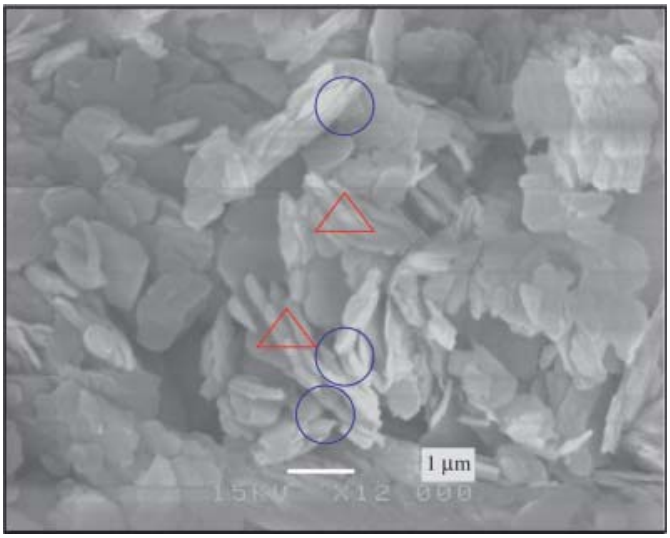

~1.10 μm, which represents the pore size inside flocculation. Its second peak in the pore-size distribution, as expected, is located around the regime where the predominant pore size of the pH 7.8 sample occurs, ~0.28 μm, which, as noted, represents the pore size in the FF association.

The SEM images and the results of pore-size distributions demonstrate a distinct dual-porosity characteristic in the pH 4 with salts specimen. It consists not only of inter-aggregate spaces enclosed by flocculation, but also intra-aggregate pores embedded in the FF association. Once again, it is worthwhile to note that the intra-aggregate pore size (measured value ~300 nm) may not be necessarily limited by the distance for the double-layer forces to act across, ~10 nm, as suggested by Griffiths and Joshi (1991).

Atterberg limits

Table 5 summarizes the liquid limit (LL), plastic limit (PL), and plasticity index (PI) of the specimens with different fabrics. Under the electrolyte-free condition, LL increases with decreasing pH, suggesting soils with higher degrees of EF flocculation can give rise to a higher LL. This observation is further confirmed by comparing the specimens with additional salt. In the presence of NaCl electrolytes (0.15 mol/L), the LL of the pH 4 specimen decreases in response to the deconstruction of the EF structure; however, the LL of the pH 7.8 specimen increases because of augmented flocculated fabrics. Similar explanations can be found in earlier studies (Sridharan et al. 1988; Sridharan and Prakash 1998): soils with a higher degree of particle flocculation can enclose larger void space for water entrapment and therefore exhibit a higher LL. Nevertheless, this discussion cannot complete the whole picture regarding the underlying mechanisms of the LL and is unable to explain the soil response during the measurement by the cone penetrometer method on the same specimen: the penetration depth is regulated by adjusting water contents.

There are possibly three main shear resistances that contribute to the shear strength of soil at the liquid limit water

Fig. 13. Pore-size distributions for the specimens with two different fabrics: (*a*) cumulative intruded volumes versus pore diameter; (*b*) intruded volume versus pore diameter.

(a)

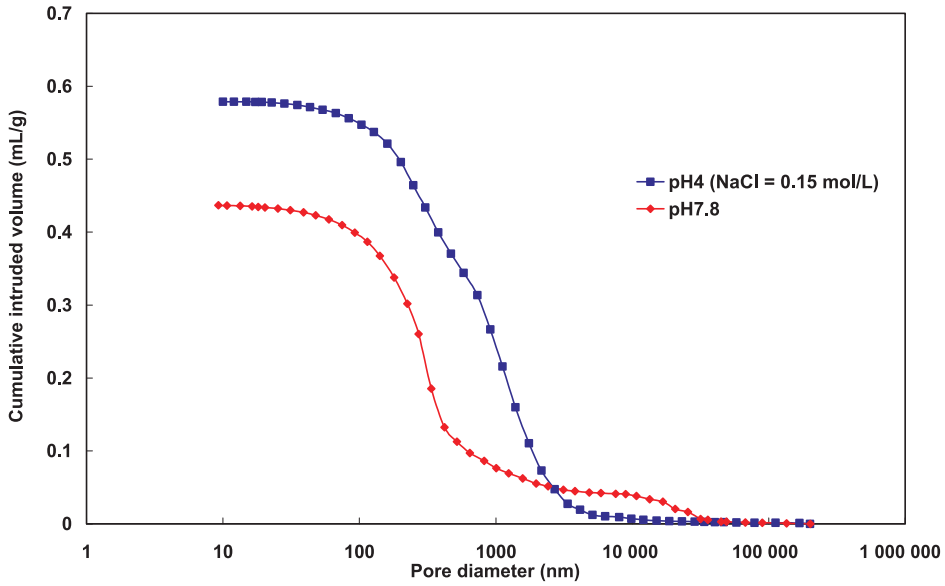

(b)

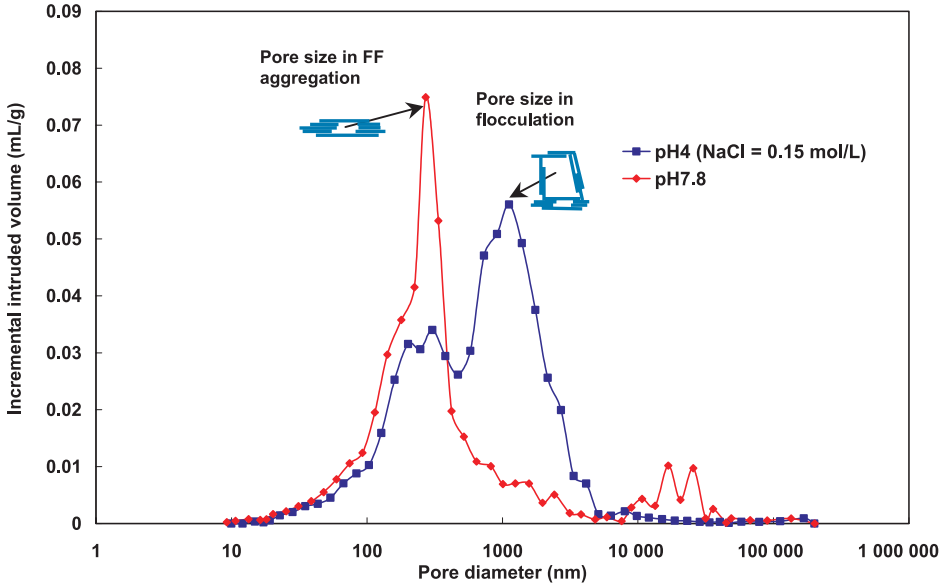

Table 5. Atterberg limits of kaolinite soils with different fabrics.

	pH 3	pH 4	pH 4[a]	pH 5	pH 7	pH 7.8	pH 7.8[a]
Liquid limit (%)	69.4	62.7	60.5	57.9	45.9	47.1	59.8
Plastic limit (%)	33.8	34.5	29.3	29.7	30.0	30.7	29.4
Plasticity index (%)	36.0	28.2	31.2	28.2	15.9	16.4	30.4

[a]Sample with salt concentration of 0.15 mol/L.

content, τ_{LL}, namely the resistance arising from the particle friction, $\tau_{friction}$, that due to interparticle electrical forces (attraction minus repulsion) τ_{A-R}, and that caused by soil suction $\tau_{suction}$. That is,

$$[5] \qquad \tau_{LL} = \tau_{friction} + \tau_{A-R} + \tau_{suction}$$

With similar τ_{LL} (same cone penetrating the same depth) and $\tau_{friction}$ (same minerals), the lowered $\tau_{suction}$ due to increasing water content (i.e., a higher LL) can be compensated by a greater τ_{A-R} from stronger interparticle attractive forces. EF flocculation is formed while the Coulombian attraction dominates at pH < IEP_{edge}, or while the van der Waals attraction prevails at pH > IEP_{edge} under the addition of electrolytes. The formation of EF flocculation implies stronger interparticle attractive forces, and therefore the measured LL is correspondingly higher. An argument against this explanation might be raised because published results demonstrate that the LL of expansive clays, such as montmorillonite, varies in an opposite way: decreasing the thickness of the double layer (i.e., increasing the interparticle attractive force) leads to a lower LL (e.g., Ridley et al. 1984). Indeed, this discrepancy can be attributed to the large quantity of interlayer water, which plays an important role in interlayer swelling and effectively in increasing the water content. Increasing the cation concentration or valence not only increases the interparticle force, which is supposed to increase the LL following the previous elucidation, but also shrinks the double-layer thickness between layers, which in turn decreases the water content and the LL. The latter part in general dominates because a montmorillonite particle contains many layers that occupy a huge portion of the specific surfaces of the particles (Santamarina et al. 2002). This discussion also reveals that eq. [5] and associated explanations cannot explain the complete LL scenario in expansive clay unless interlayer water is taken into account.

The plastic limit, however, does not show any obvious trend in response to different pH and electrolyte concentrations. The value for all soil samples is around 30, which in turn shows that soils with higher LL also demonstrate a greater plasticity index, PI.

Summary and concluding remarks

The portion of edge surfaces in kaolinite is high, and the face charge in kaolinite because of isomorphic substitution is not severe. Consequently, the pH-dependent edge charges impact the interparticle force and associated fabric formations of kaolinite. As shown in the sedimentation test, the EF Coulombian attraction prevails at low pH because the edge site becomes positive due to protonation in the acidic environment. Such an EF association leads to a higher initial settling rate and a voluminous final sediment volume. At high pH, particle coagulation is prevented due to strong interparticle repulsion because all surfaces (faces and edges) are negatively charged. The initial settling rate and the final sediment volume are therefore correspondingly lower. A distinct transition point, pH 5, can be found as a boundary to separate the high and low pH. This pH boundary also can be simply estimated as the isoelectric point of edge surfaces, IEP_{edge}, for the kaolinite studied herein. In the presence of electrolytes (NaCl), the behavior of suspensions with a pH below or above the IEP_{edge} is completely the opposite. At pH < IEP_{edge}, increasing the ionic strength (NaCl) disrupts the EF association because of a reduction in the Coulombian attraction. Therefore, a decreasing trend in the final sediment volume with an increase in the ionic strength can be measured. At pH > IEP_{edge}, however, adding NaCl promotes a higher degree of flocculation (also aggregation) because the double layers are compressed at all surfaces and van der Waals attraction prevails for particle coagulation to form a bulk sediment.

The measured pore-size distribution and SEM images of kaolinite specimens with different fabrics are consistent with the conclusion obtained from the sedimentation test. This reveals that the fabric formed during deposition can be sustained after the one-dimensional (1D) consolidation of 100 kPa. The predominant pore size of the pH 4 with 0.15 mol/L NaCl specimen is around 1.10 μm, which corresponds to the interaggregate spaces enclosed with the EF flocculation. For the specimens at pH 7.8, the main pore size is around 0.30 μm, suggesting the intra-aggregate pore dimension embedded in the FF association. Such an intra-aggregate pore size is much larger than the distance that the double layer can act across, ~10 nm, because the FF association is not uniformly packed. The irregularities of particle shapes, sizes, packing, and orientation certainly help enlarge the pore size within the FF association. Moreover, the results of the pore-size distribution reveal a distinct dual-porosity characteristic for the pH 4 with 0.15 mol/L NaCl specimen. The results of the liquid limit (LL) tests suggest that the LL of kaolinite increases with an increase in interparticle force: the higher degree of EF flocculation due to Coulombian or van der Waals attraction can render a higher LL. There is no clear trend observed for the plastic limit, however.

Acknowledgements

This research was supported by the Research Grants Council (HKUST6034/02E), Hong Kong. The authors are grateful to the reviewers for valuable comments.

References

ASTM. 1995. Standard test method for liquid limit, plastic limit, and plasticity index for soils (D4318-95a). *In* 1997 Annual Book of ASTM Standards. American Society for Testing and Materials (ASTM), Philadelphia, Penn. Vol. 04.08, Soil and Rock (I), pp. 522–532.

Bolland, M.D.A., Posner, A.M., and Quirk, J.P. 1980. pH-independent and pH-dependent surface charges on kaolinite. Clays and Clay Minerals, **28**: 412–418.

Brady, P.V., Cygan, R.T., and Nagy, K.L. 1996. Molecular controls on kaolinite surface charge. Journal of Colloid Interface Science, **183**: 356–364.

Braggs, B., Fornasiero, D., Ralston, J., and Smart, R.S. 1994. The effect of surface modification by an organosilane on the electrochemical properties of kaolinite. Clays and Clay Minerals, **42**(2): 123–136.

British Standards Institution. 1990. Methods of test for soils for civil engineering purposes (BS1377). British Standards Institution, London, UK.

Broderick, G.P., and Daniel, D.E. 1990. Stabilizing compacted clay against chemical attack. Journal of Geotechnical Engineering, ASCE, **116**(10): 1549–1567.

Carty, W.M. 1999. The colloidal nature of kaolinite. American Ceramic Society Bulletin, **78**(8): 72–76.

Chamley, H. 1989. Clay sedimentology. Springer-Verlag, New York.

Chen, J., and Anandarajah, A. 1998. Influence of pore fluid composition on volume of sediments in kaolinite suspensions. Clays and Clay Minerals, **46**(2): 145–152.

Chen, J., Anandarajah, A., and Inyang, H. 2000. Pore fluid properties and compressibility of kaolinite. Journal of Geotechnical and Geoenvironmental Engineering, ASCE, **126**(9): 798–807.

Dollimore, D., and Horridge, T.A. 1972. The dependence of the flocculation behavior of china clay polyacrylamide suspension on the suspension pH. Journal of Colloid and Interface Science, **42**(3): 581–588.

Evans, J.C. 1990. Geotechnics of hazardous waster control systems. *In* Foundation engineering handbook. *Edited by* H.Y. Fang. 2nd ed. Van Nostrand Reinhold, New York. pp. 750–777.

Fam, M., and Dusseault, M. 1998. Evaluation of surface-related phenomena using sedimentation tests. Geotechnical Testing Journal, **21**(3): 180–184.

Fernandez, F., and Quigley, R.M. 1985. Hydraulic conductivity of natural clays permeated with simple liquid hydrocarbons. Canadian Geotechnical Journal, **22**: 205–214.

Ferris, A.P., and Jepson, W.B. 1975. The exchange capacities of kaolinite and the preparation of homoionic clays. Journal of Colloid Interface Science, **51**: 245–259.

Flegmann, A.W., Goodwin, J.W., and Ottewill, R.H. 1969. Rheological studies on kaolinite suspensions. Proceedings of the British Ceramic Society, **31**: 31–45.

Griffiths, F.J., and Joshi, R.C. 1989. Change in pore size distribution due to consolidation of clays. Géotechnique, **39**: 159–167.

Griffiths, F.J., and Joshi, R.C. 1991. Change in pore size distribution owing to secondary consolidation of clays. Canadian Geotechnical Journal, **28**(1): 20–24.

Hicher, P.Y., Wahyudi, H., and Tessier, D. 2000. Microstructural analysis of inherent and induced anisotropy in clay. Mechanics of Cohesive–Frictional Materials, **5**: 341–371.

Huang, C.P., and Stumm, W. 1973. Specific adsorption of cations on hydrous γ-Al_2O_3. Journal of Colloid and Interface Science, **43**(2): 409–420.

Hurlbut, C.S.J. 1971. Dana manual of mineralogy. 18th ed. John Wiley and Sons, New York.

Jepson, W.B. 1984. Kaolins: their properties and uses. Philosophical Transactions of the Royal Society of London, **311**: 411–432.

Kretzschmar, R., Holthoff, H., and Sticher, H. 1998. Influence of pH and humic acid on coagulation kinetics of kaolinite: a dynamic light scattering study. Journal of Colloid and Interface Science, **202**: 95–103.

Lambe, T.W. 1958. The structure of compacted clay. Journal of the Soil Mechanics and Foundations Division, ASCE, **82**(2): 1654-1–1654-34.

Low, P.F. 1991. Interparticle forces in clay suspensions: flocculation, viscous flow and swelling. *In* Proceedings of the 1989 Clay Minerals Society Workshop on the Rheology of Clay/Water System. Clay Minerals Society, Boulder, Colo. pp. 158–189.

Ma, C., and Eggleton, R.A. 1999. Cation exchange capacity of kaolinite. Clays and Clay Minerals, **47**(2): 174–180.

Ma, K., and Pierre, A.C. 1999. Clay sediment–structure formation in aqueous kaolinite suspensions. Clays and Clay Minerals, **47**(4): 522–526.

Mitchell, J.K. 1993. Fundamentals of soil behavior. 2nd ed. John Wiley & Sons, Inc., New York.

Parks, G.A. 1967. Aqueous surface chemistry of oxides and complex oxide minerals; isoelectric point and zero point of charge. *In* Equilibrium concepts in natural water systems. *Edited by* W. Stumm. Advances in Chemistry Series, No. 67, American Chemistry Society, Washington, DC. pp. 121–160.

Penumadu, D., and Dean, J. 2000. Compressibility effect in evaluating the pore-size distribution of kaolin clay using mercury intrusion porosimetry. Canadian Geotechnical Journal, **37**(2): 393–405.

Plancon, A., Giese, R.F., Jr., Snyder, R., Drits, V.A., and Bookin, A.S. 1989. Stacking faults in the kaolin-group minerals: deflect structures of kaolinite. Clays and Clay Minerals, **37**(3): 203–210.

Rand, B., and Melton, I.E. 1977. Particle interaction in aqueous kaolinite suspensions I. Effect of pH and electrolyte upon the mode of particle interaction in homoionic sodium kaolinite suspensions. Journal of Colloid and Interface Science, **60**(2): 308–320.

Rhoades, J.D. 1996. Salinity: electrical conductivity and total dissolved solids. *In* Methods of soil analysis. Part 3. Chemical methods. *Edited by* J.M. Bigham. Soil Science Society of America, Inc., Madison, Wis. pp. 417–435.

Ridley, K.J.D., Bewtra, J.K., and McCorquodale, J.A. 1984. Behavior of compacted fine-grained soils in a brine environment. Canadian Journal of Civil Engineering, **11**: 196–203.

Santamarina, J.C., and Fam, M. 1995. Changes in dielectric permittivity and shear wave velocity during concentration diffusion. Canadian Geotechnical Journal, **32**(4): 647–659.

Santamarina, J.C., Klein, K.A., and Fam, M.A. 2001. Soils and waves. John Wiley & Sons Ltd., New York.

Santamarina, J.C., Klein, K.A., Wang, Y.H., and Prencke, E. 2002. Specific surface: determination and relevance. Canadian Geotechnical Journal, **39**(1): 233–241.

Schofield, R.K., and Samson, H.R. 1954. Flocculation of kaolinite due to the attraction of oppositely charged crystal faces. Faraday Society Discussions, **18**: 138–145.

Sposito, G. 1998. On points of zero charge. Environment Science and Technology, **32**: 2825–2819.

Sridharan, A., and Prakash, K. 1998. Characteristic water contents of a fine-grained soil–water system. Géotechnique, **48**(3): 337–346

Sridharan, A., and Rao, V.G. 1979. Shear strength behavior of saturated clays and the role of effective stress concept. Géotechnique, **29**(2): 177–193.

Sridharan, A., Rao, S.M., and Murthy, N.S. 1988. Liquid limit of kaolinitic soils. Géotechnique, **38**(2): 191–198.

Stumm, W. 1992. Chemistry of the solid–water interface. John Wiley and Sons, Inc., New York.

Toorman, E.A. 1996. Sedimentation and self-weight consolidation: general unifying theory. Géotechnique, **46**(1): 103–113.

van Olphen, H. 1991. An introduction to clay colloid chemistry: for clay technologists, geologists and soil scientists. Reprint version. John Wiley and Sons, Inc., New York.

Washburn, E.W. 1921. A note on a method of determining the distribution of pore sizes in a porous material. Proceedings of the National Academy of Science, **7**: 115–116.

Wierer, K.A., and Dobias, B. 1988. Exchange enthalpies of H^+ and OH^- adsorption on minerals with different characters of potential-determining ions. Journal of Colloid Interface Science, **122**: 171–177.

Yao, M., and Anandarajah, A. 2003. Three-dimensional discrete element method of analysis of clays. Journal of Engineering Mechanics, **129**(6): 585–596.

Zbik, M., and Smart, R.S.C. 1998. Nanomorphology of kaolinites: comparative SEM and AFM studies. Clays and Clay Minerals, **46**(2): 153–160.

Zhou, Z.H., and Gunter, W.D. 1992. The nature of the surface charge of kaolinite. Clays and Clay Minerals, **40**(3): 365–368.